Polymer Chemistry

ROYAL SOCIETY OF CHEMISTRY

PAPER

View Article Online
View Journal | View Issue

Cite this: *Polym. Chem.*, 2022, **13**, 6046

Enhancing intrinsic thermal conductivities of epoxy resins by introducing biphenyl mesogen-containing liquid crystalline co-curing agents†

Jinjin Dang,[a,b] Junliang Zhang, *[a,b] Mukun Li,[c] Lin Dang[a,b] and Junwei Gu*[a,b]

Received 7th September 2022,
Accepted 9th October 2022

DOI: 10.1039/d2py01157c

rsc.li/polymers

In this work, a biphenyl liquid crystalline small molecule (BLCM) containing flexible units was synthesized *via* a one-step condensation reaction of 4,4′-dihydroxybiphenyl (BP) and 1,6′-dibromohexene. Then, the commercially available bisphenol A epoxy (E-51) was used as a matrix, 4,4′-diaminodiphenylmethane (DDM) as a curing agent, and the BLCM as a co-curing agent to prepare highly intrinsic thermally conductive liquid crystalline epoxy resins (LCER) by a casting method. Nuclear magnetic resonance spectroscopy, high-resolution mass spectroscopy, and Fourier transform infrared spectroscopy demonstrated that the BLCM with a designed structure was synthesized successfully. Wide-angle X-ray diffraction, small-angle X-ray scattering, and polarized light microscopy proved that the inter-stacking of biphenyl mesogens promoted the formation of locally ordered regions in the LCER. Meanwhile, the ordered structure of the LCER was enhanced with an increase of the BLCM mass fraction, resulting in the higher intrinsic thermal conductivity. When the mass fraction of the BLCM was 60% of E-51 (LCER3), the thermal conductivity (λ) of LCER3 was 0.42 W (m K)$^{-1}$, which was 2.1 times that of an epoxy resin cured with DDM only (LCER0, λ was 0.20 W (m K)$^{-1}$). Besides, LCER3 presented a high heat resistance index (T_{HRI}) of 176.8 °C, elastic modulus of 4.8 GPa, and hardness of 0.32 GPa, which was also higher than LCER0 with a T_{HRI} of 172.2 °C, elastic modulus of 3.7 GPa, and hardness of 0.27 GPa.

1. Introduction

Epoxy resins account for approximately 70% of the entire thermosetting resin market, having been widely applied in the fields of electronics, electrical engineering, and electronic packaging due to their excellent electrical insulation properties, mechanical properties, chemical resistance, and easy processability.[1–3] With the rapid development of electronic and electrical components towards miniaturization, high integration, and high power,[4–6] the heat accumulation during operation of equipment is inevitably becoming more and more serious.[7,8] However, conventional epoxy resins form disordered cross-linked structures after curing, causing serious phonon scattering inside the cured resin network. Therefore, epoxy resins generally present low intrinsic thermal conductivity (λ) of only about 0.2 W (m K)$^{-1}$.[9–11]

Currently, the incorporation of thermally conductive fillers, such as metals,[12–14] carbon,[15–17] and ceramics[18–20] into epoxy resins is commonly applied to prepare epoxy composites with enhanced thermal conductivities. Although the preparation process is relatively simple, the effect of improving the thermal conductivity is not ideal when the content of fillers is low as a thermal conduction path cannot be formed.[21,22] While bringing an enhancement of the thermal conductivity by further increasing the amount of thermally conductive fillers, they inevitably cause adverse effects on the mechanical strength, flexibility, optical transparency, and processability of epoxy composites, and seriously threaten their service life and reliability.[23–25] Meanwhile, researchers have shown that the thermal conductivity of polymer composites, to a large degree, depend on the polymer matrix rather than the thermally conductive fillers.[26] In this regard, increasing the intrinsic thermal conductivity of epoxy resin by suppressing phonon scattering within the cured resin network through improving the microscopic order provides a feasible solution.[27,28]

Researchers generally introduce mesogenic units into the molecular structure of epoxy monomers, which form a local crystal-like structure within the cured network after curing. Therefore, the ordered microstructure that is formed reduces molecular defects and improves the coordination of molecular vibrations and lattice vibrations, which suppresses the phonon scattering and increases the mean-free path of phonons, thus

[a]*Research & Development Institute of Northwestern Polytechnical University in Shenzhen, Shenzhen 518057, P. R. China. E-mail: junliang.zhang@nwpu.edu.cn, gjw@nwpu.edu.cn, nwpugjw@163.com*
[b]*Shaanxi Key Laboratory of Macromolecular Science and Technology, School of Chemistry and Chemical Engineering, Northwestern Polytechnical University, Xi'an 710072, Shaanxi, P. R. China*
[c]*Queen Mary University of London Engineering School, NPU, Northwestern Polytechnical University, Xi'an 710072, Shaanxi, P. R. China*
† Electronic supplementary information (ESI) available. See DOI: https://doi.org/10.1039/d2py01157c

improving the intrinsic thermal conductivity of the epoxy resin.[29,30] For instance, Lin *et al.*[31] synthesized a liquid crystalline epoxy monomer with ketone mesogens using *p*-hydroxybenzaldehyde, acetone, and epichlorohydrin as the main raw materials. The λ of the cured epoxy resin reached 0.34 W (m K)$^{-1}$ with 4,4′-diaminodiphenylmethane (DDM) as the curing agent. Zhang *et al.*[32] synthesized a liquid crystalline epoxy monomer containing the biphenyl mesogenic unit applying 4,4′-dihydroxybiphenyl and 6-bromo-1-hexene and the λ of cured resin reached 0.31 W (m K)$^{-1}$. In our previous works, Gu *et al.*[33] synthesized a triphenylene-based discotic liquid crystalline epoxy monomer from catechol, ethylene glycol monoallyl ether, and chloroperoxybenzoic acid. The epoxy resin cured with DDM showed enhanced intrinsic thermal conductivity with a λ in the vertical direction ($\lambda_\perp$) of 0.35 W (m K)$^{-1}$ and in the parallel direction ($\lambda_\parallel$) of 1.37 W (m K)$^{-1}$. Furthermore, Gu *et al.*[34] synthesized a side-chain liquid crystalline epoxy monomer based on biphenyl liquid crystalline units and employed curing agents with ester bonds containing thiols. Enhanced intrinsic thermal conductivity was achieved with $\lambda_\perp$ of 0.33 W (m K)$^{-1}$ and $\lambda_\parallel$ of 1.25 W (m K)$^{-1}$. However, complicated synthetic steps and tedious purification processes to synthesize liquid crystalline epoxy monomers are always required, resulting in a low final yield and high cost from the perspective of practical applications, which circumvents their wide use.

In addition to synthesizing liquid crystalline epoxy monomers, introducing mesogenic units into the curing/co-curing agent can also improve the microscopic order of the cured epoxy resin network, which effectively reduces phonon scattering and thus improves the intrinsic thermal conductivity.[35–37] Besides, the synthesis of a liquid crystalline curing/co-curing agent is relatively simple compared to the synthesis of liquid crystalline epoxy monomers. However, preparing epoxy resins with enhanced intrinsic thermal conductivity using liquid crystalline curing/co-curing agents has rarely been investigated and reported to date. In the present work, we report the synthesis of a liquid crystalline co-curing agent and its application to prepare epoxy resins with enhanced intrinsic thermal conductivity. It is expected to provide a relatively facile and convenient approach for the preparation of highly intrinsic thermally conductive epoxy resins.

Herein, a biphenyl mesogen-containing liquid crystalline co-curing agent, 4′,4‴-(hexane-1,6-diylbis(oxy))bis(([1,1′-biphenyl]-4-ol)) (BLCM) with flexible segments, was synthesized by a one-step condensation reaction of 4,4′-dihydroxybiphenyl (BP) and 1,6′-dibromohexene. 4,4′-diaminodiphenylmethane (DDM) and BLCM were then employed as curing/co-curing agents to cure the commercially available bisphenol A epoxy (E-51) to prepare liquid crystalline epoxy resins (LCER, Scheme 1) with enhanced intrinsic thermal conductivity by casting. ^{1}H and ^{13}C nuclear magnetic resonance (^{1}H NMR and ^{13}C NMR), high-resolution mass spectroscopy (HRMS), Fourier transform infrared (FT-IR) spectroscopy, hot-stage polarized light microscopy (POM), and differential scanning calorimetry (DSC) were performed during the analysis and characterization of the structure and liquid crystalline properties of BLCM. The curing process and microstructure of the LCER were characterized by FT-IR, DSC, wide-angle X-ray diffraction (WAXD), small-angle X-ray scattering (SAXS), and POM. The effects of the mass fraction of BLCM on the thermal conductivity, heat resistance, and mechanical properties of the LCER were investigated.

2. Experimental part

2.1. Synthesis of BLCM

BP (4.7 g, 25 mmol), KOH (0.56 g, 10 mmol), and ethanol (300 mL) were introduced into a 500 mL three-necked round bottom flask and stirred evenly. 1,6′-dibromohexane (1.22 g, 5 mmol) was then added to the above solution and heated to reflux at 85 °C for 24 h. The solvent was then removed by suction filtration. The obtained solid was washed 3 times using 300 mL of ethanol and 300 mL of distilled water, respectively, and dried at 60 °C for 24 h under a vacuum. The product was acidified with hydrochloric acid (1 mol L^{-1}) and washed with distilled water 3 times, then dried at 60 °C for 24 h under a vacuum to afford BLCM with a yield of 89.4%.

2.2. Preparation of the LCER

A certain amount of BLCM, DDM, and E-51 (0 : 25 : 100, 20 : 21 : 100, 40 : 17 : 100 and 60 : 12 : 100, wt/wt/wt, with the stoichiometric ratio of hydroxyl groups and amine groups to epoxy groups being 1 : 1) were mixed and heated to 80 °C to melt with stirring. The mixture was then poured into a preheated mold at 80 °C, degassed under a vacuum, and cured at 185 °C for 6 h to obtain the LCER (where samples are denoted as LCER0, LCER1, LCER2, and LCER3, respectively).

3. Results and discussion

3.1. Structural characterizations of BLCM

BLCM was firstly characterized by ^{1}H NMR (Fig. 1a) and ^{13}C NMR (Fig. 1b) spectroscopy. The peaks at 9.4 ppm and 6.8–7.5 ppm in Fig. 1a correspond to the protons of the hydroxyl groups and benzene ring, respectively. The protons with the chemical shift of 4.0, 1.7, and 1.5 ppm are attributed to the methylene groups of the flexible segment in BLCM. Besides, the integration ratio of the peaks a : (c + d) : (b + e) : f : g : h is 1 : 4 : 4 : 2 : 2 : 2, which is consistent with the molecular structure of BLCM. Additionally, the ^{13}C NMR spectrum of BLCM reveals the carbon atoms on the benzene ring at 157.9, 157.1, 133.1, 130.9, 116.1, and 115.2 ppm. Furthermore, the peaks at 67.8, 29.1, and 25.7 ppm are associated with the carbon atoms of the methylene groups. HRMS (Fig. S1†) was also performed, which reveals that the *m*/*z* calculated for $C_{30}H_{29}O_4$ ($[M - H]^+$) is 453.21 and the *m*/*z* found is 453.20682. FT-IR spectroscopy was also conducted for BLCM. As shown in Fig. S2,† the stretching vibration peak of the phenolic hydroxyl group appears at 3374 cm^{-1} while the peak at 2864–2960 cm^{-1}

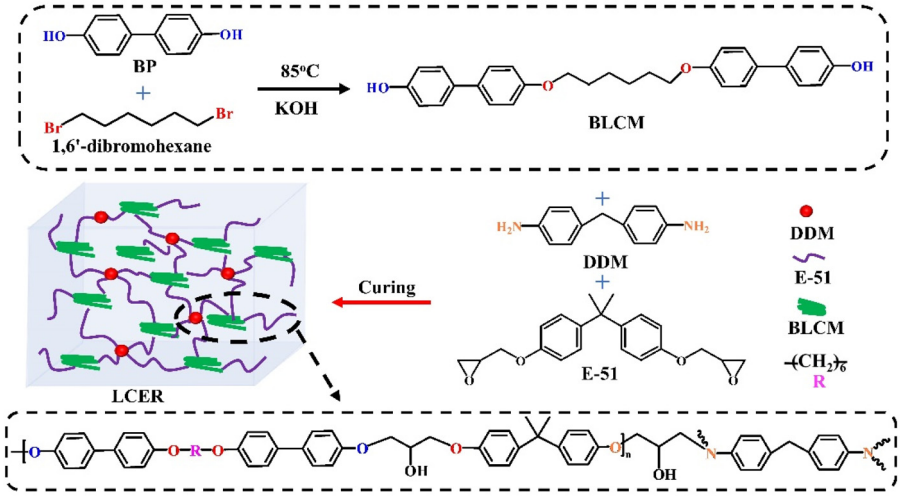

Scheme 1 Schematic diagram of the synthetic route of BLCM and LCER.

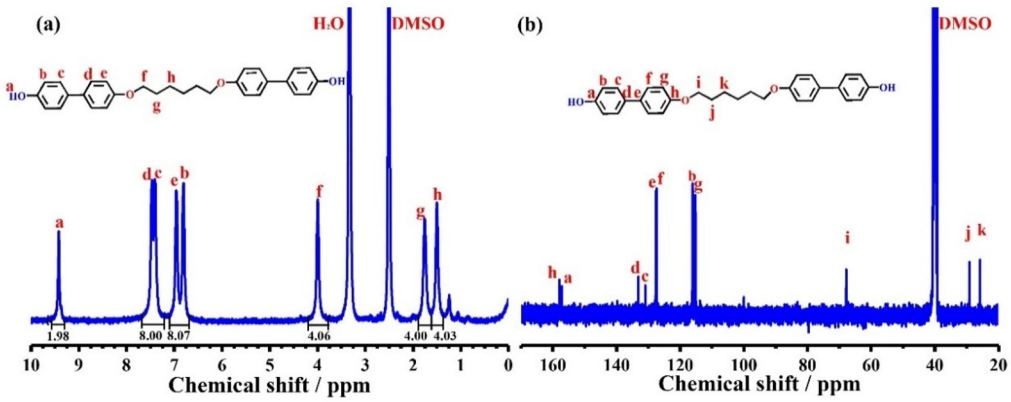

Fig. 1 (a) ^{1}H NMR and (b) ^{13}C NMR spectra of BLCM.

is attributed to the stretching vibration of methylene. In addition, the stretching vibration peak of the ether bond is present at 1041 cm^{-1}. The peak at 812 cm^{-1} corresponds to the stretching vibration of the *para*-substituted benzene ring. These results suggest the successful synthesis of BLCM with the designed structure.

3.2. Liquid crystalline behavior of BLCM

The liquid crystalline behavior of BLCM was characterized by DSC and POM. Based on the DSC curves (Fig. 2a), two peaks appear in both the heating and cooling processes of BLCM. During the heating process, two endothermic peaks appear at 244 °C and 256 °C, respectively. The first one corresponds to the transition of BLCM from the crystalline phase to a liquid crystalline phase, while the second one indicates the transition from the liquid crystalline phase to an isotropic phase. The exothermic peak at 222 °C during the cooling process indicates the isotropic phase to the liquid crystalline phase transition while the exothermic peak at 211 °C represents the transformation from the liquid crystalline phase to the crystalline phase.

Meanwhile, it can be seen from the POM images (Fig. 2b) that BLCM is solid at room temperature and shows no liquid crystallinity. As the temperature increases to 245 °C, the visual area turns brighter and BLCM exhibits fluidic behavior, indicating the liquid crystalline state. When the temperature is further increased to 251 °C, bright yellow spots cover the entire visual field, which disappear completely as the temperature continues rising to 265 °C. During the cooling process, the bright yellow spots gradually appear once again, when the temperature decreases to 224 °C, and continue to spread over the whole visual field with a decreasing of the temperature to 215 °C, and then disappear completely as BLCM was cooled to room temperature. The POM and DSC analyses show consistent results, indicating that BLCM presents bidirectional thermotropic liquid crystalline properties.

3.3. Curing behaviors of LCERs

The curing processes of LCERs were firstly analyzed by FT-IR spectroscopy. As can be seen from Fig. 3, the intensities for both the peaks of epoxy groups at 910 cm^{-1} and phenolic

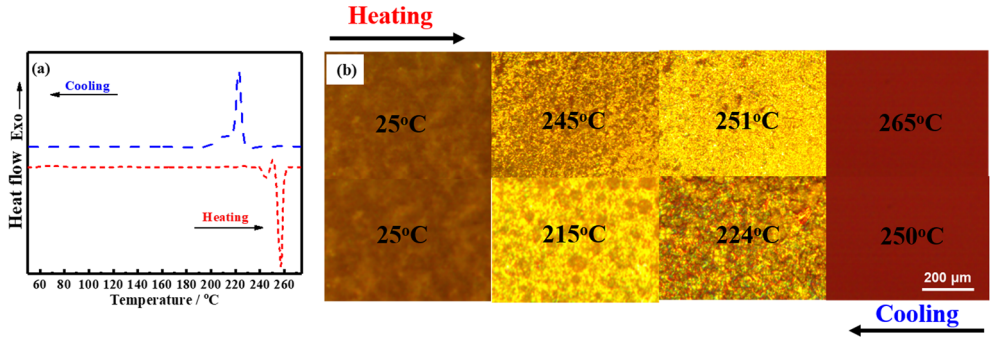

Fig. 2 (a) DSC curves and (b) POM images during the heating and cooling processes of BLCM.

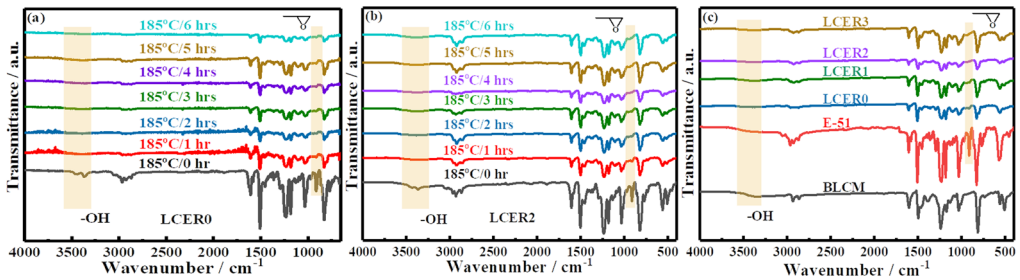

Fig. 3 FT-IR spectra of (a) LCER0 and (b) LCER2 at different time during the curing process; (c) FT-IR spectra of cured LCERs, E-51, and BLCM.

hydroxyl groups of BLCM and hydroxyl groups of E-51 at 3374 cm^{-1} are gradually weakened as curing progresses for LCER0 (Fig. 3a; see Fig. S3a† for the zoomed-in FT-IR spectra of the fingerprint region) and LCER2 (Fig. 3b; see Fig. S3b† for the zoomed-in FT-IR spectra of the fingerprint region). It takes 6 hours for the characteristic peak of epoxy groups to disappear completely in LCER0 while it takes only 4 hours for LCER2, indicating a faster curing rate in LCER2 than LCER0. Besides, as observed in Fig. 3c (see Fig. S3c† for the zoomed-in spectra of the fingerprint region), LCER1 and LCER3 exhibit the same characteristic peaks as seen for LCER2, showing the complete disappearance of epoxy groups at 910 cm^{-1} and the nearly complete disappearance of hydroxyl groups at 3374 cm^{-1}. The remaining signal at 3374 cm^{-1} is attributed to the hydroxyl groups formed by the ring-opening of epoxy groups. These findings prove that both BLCM and DDM have participated in the curing reactions of E-51.[38]

The curing processes of different LCERs were further investigated by non-isothermal DSC (Fig. S4†) at 10 °C min^{-1}. It can be seen that the exothermic peaks gradually broaden while the peak temperature (T_p, Table S1†) shifts toward lower values gradually with an increasing mass fraction of BLCM. The T_p of the exothermic peak for LCER3 is 144.8 °C, which is 22.5 °C lower than that of LCER0 (167.3 °C). It suggests that the curing process is relatively mild and BLCM promotes the curing of E-51. This is because BLCM introduces mesogenic units into the curing networks of epoxy resin, which increases the regularity and overall order of the microstructure. Therefore, the intermolecular interactions are enhanced, and the curing reaction is accelerated, leading to the decreased T_p value of the curing exothermic peak.[39] This result is consistent with the real-time infrared analysis.

The curing processes were also investigated using DSC with different heating rates of 5 °C min^{-1}, 10 °C min^{-1}, 15 °C min^{-1}, and 20 °C min^{-1} for each LCER (Fig. S5,† peak temperatures shown in Table S1†). DSC reveals that T_p increases with increasing heating rate for the same LCER. This is because an acceleration of the heating rate increases the heat flow per unit time, resulting in a greater thermal effect. This effect accumulates over the entire heating process, causing the shift of exothermic peak toward higher temperatures. Based on the peak temperatures from the DSC analyses at different heating rates, the curing kinetic curves and the corresponding apparent activation energy for each LCER obtained by the Kissinger method (eqn (S1)†) and the Ozawa method (eqn (S1)†) are shown in Fig. S6 and Table S2,† respectively.[40,41]

It can be seen that the apparent activation energy gradually decreases with an increase of the BLCM mass fraction. The apparent activation energies of LCER3 calculated by the Kissinger method and Ozawa method are 49.4 kJ mol^{-1} and 53.4 kJ mol^{-1}, respectively, which are 16.4% and 15.2% lower than those of LCER0 (57.5 kJ mol^{-1} and 61.5 kJ mol^{-1}), respectively. These findings further prove that BLCM accelerates the curing of E-51.

3.4. Thermal conductivities of LCERs

The thermal conductivities of LCERs were measured by a thermal constant analyzer. As shown in Fig. 4a, the λ of LCERs

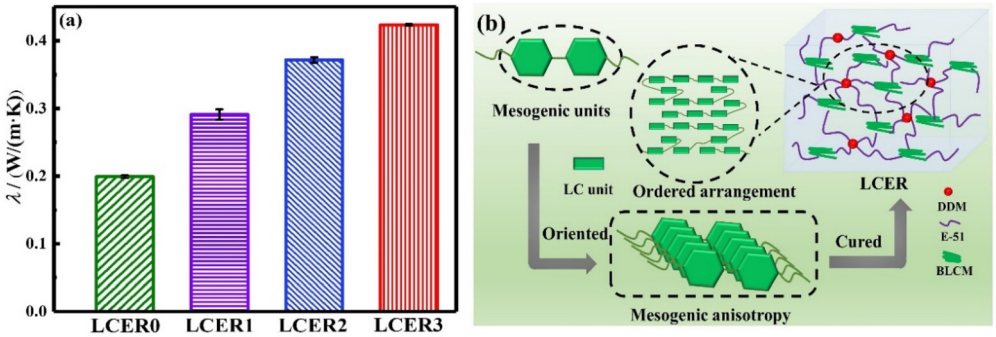

Fig. 4 (a) Thermal conductivities (λ) of LCERs; (b) schematic diagram of a mesomorphic phase arrangement within the cured epoxy network.

gradually increases when increasing the proportion of BLCM. The λ of LCER3 increases to a maximum of 0.42 W (m K)$^{-1}$, which is 2.1 times that of LCER0 with λ of 0.20 W (m K)$^{-1}$. This is attributed to the stacked structure formed by the biphenyl mesogens of BLCM, resulting in fixed microscopically ordered regions consisting of mesogenic units within the cured epoxy network. Besides, the π–π stacking interaction between biphenyl units can suppress the random orientation of molecular chains and promote the formation of a layered and ordered microstructure (Fig. 4b), which suppresses phonon scattering, thereby enhancing the intrinsic thermal conductivity.[42]

In order to further explore the influential factors and mechanism of the enhanced intrinsic thermal conductivity, WAXD, SAXS, and POM were employed to characterize the LCERs. As shown in Fig. 5a, the WAXD curve of LCER0 exhibits no sharp diffraction peaks but only a broad diffuse peak. This suggests that only a disordered structure was formed within the cured network of LCER0. WAXD curves of LCER1, LCER2, and LCER3, on the other hand, all display six distinct sharp diffraction peaks at 2θ = 2.60°, 4.72°, 19.09°, 20.55°, 23.99°, and 29.55°, 2θ = 3.10°, 6.21°, 18.69°, 20.48°, 23.56°, and 28.93°, and 2θ = 3.03°, 6.18°, 18.72°, 20.38°, 23.53°, and 28.89°. These phenomena are in agreement with the existence of the microscopically ordered orientation of the intramolecular layer and intermolecular layer within the cured network. The interplanar spacings, calculated according to the Bragg formula,[43,44] are: 3.39, 1.87, 0.464, 0.432, 0.371, and 0.302 nm for LCER1; 2.85, 1.42, 0.474, 0.433, 0.377, and 0.308 nm for LCER2; and 2.91, 1.43, 0.473, 0.435, 0.378, and 0.309 nm for LCER3. Meanwhile, the respective diffraction peaks at 2θ = 29.55°, 28.93°, and 28.89° for LCER1, LCER2, and LCER3 indicate the formation of π–π stacking,[45] which proves the presence of ordered interlayer structures. In addition, the sharp diffraction peaks at 2θ between 2 and 10° reveal the formation of a smectic layer.[46] Furthermore, the crystallinities of LCERs gradually increase with the increase of the BLCM content applied, as the crystallinity was calculated to be 8.9%, 10.5%, and 14.4% for LCER1, LCER2, and LCER3, respectively.

In addition, the SAXS curve of LCER0 (Fig. S7†) shows no peaks of scattering, representing a uniform electron density and a homogeneously amorphous structure of the network. In contrast, LCER1, LCER2, and LCER3 present a strong scattering in their SAXS curves, demonstrating fluctuations of the electron density, which suggests the presence of regions of mesogenic unit aggregation and microphase separation.[47] The above results indicate that the microscopically ordered structure is enhanced by increasing the mass fraction of BLCM. In

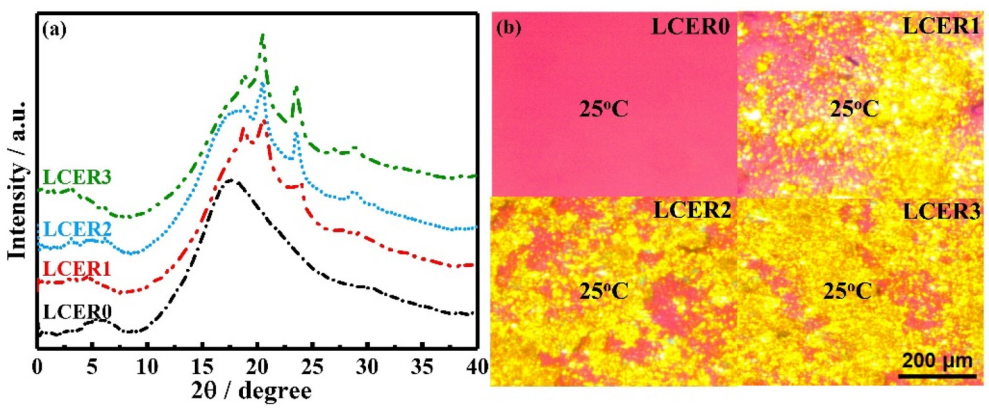

Fig. 5 (a) WAXD curves and (b) POM images of LCERs at 25 °C.

the meantime, the POM images of LCER1, LCER2, and LCER3 (Fig. 5b) exhibit birefringence and bright yellow spots spread over the visual area at room temperature, indicating the presence of a crystalline structure, which is fixed after the curing reaction. It can be concluded that the biphenyl mesogens containing the co-curing agent of BLCM improves the structural regularity of the cured epoxy network, which is positively correlated with the mass fraction of BLCM. Consequently, the intrinsic thermal conductivity is enhanced with increasing amounts of BLCM. Besides, considering the presence of the intermediate state between the crystal and amorphous states in LCER1, LCER2, and LCER3, the crystal-like structure domains of the resins will be disordered, which yields thermal conductivities that are macroscopically isotropic.

3.5. Heat resistance of LCERs

The heat resistance of LCERs was tested by TGA. As shown in Fig. 6a, the weight loss of LCERs is less than 5% before 310 °C due to their high heat resistance. Rapid decomposition occurs between 310–460 °C, caused by the destruction of the cross-linked epoxy network. Notably, the final carbon residue increases by increasing the amount of BLCM, with LCER3 being 15.7% while LCER0 is only 9.90%. As expected, the heat resistance index[48] ($T_{HRI} = 0.49 \times [T_5 + 0.6 \times (T_{30} - T_5)]$, where T_5 and T_{30} are the decomposition temperatures when the mass loss is 5% and 30%, respectively, Fig. 6b) of LCER gradually increases when increasing the mass fraction of BLCM. The T_{HRI} of LCER3 increases to the highest temperature of 176.8 °C from 172.2 °C for LCER0. This is caused by the rigid biphenyl groups in BLCM and the improvement of regularity of LCER cured networks, which restricts the thermal motion of molecular chains, thus improving the heat resistance.

3.6. Mechanical properties of LCERs

Nanoindentation was performed to characterize the indentation depth, elastic modulus, and hardness of LCERs. As shown in the load–displacement curves of LCERs (Fig. 7a), the indentation depth gradually decreases when increasing the mass fraction of BLCM. LCER3 exhibits the lowest indentation depth, indicating that the addition of BLCM improves the indentation resistance of LCERs. Moreover, both the elastic modulus and hardness of LCERs gradually increase when

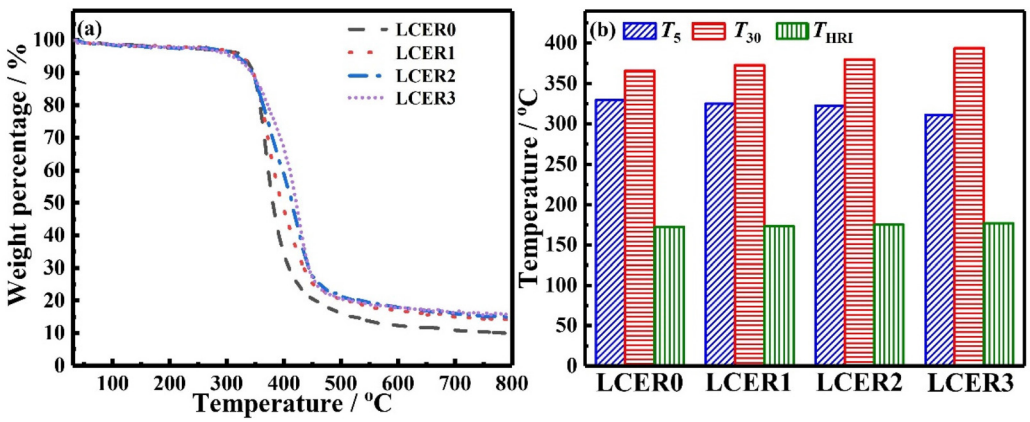

Fig. 6 (a) TGA curves and (b) characteristic thermal data of LCERs.

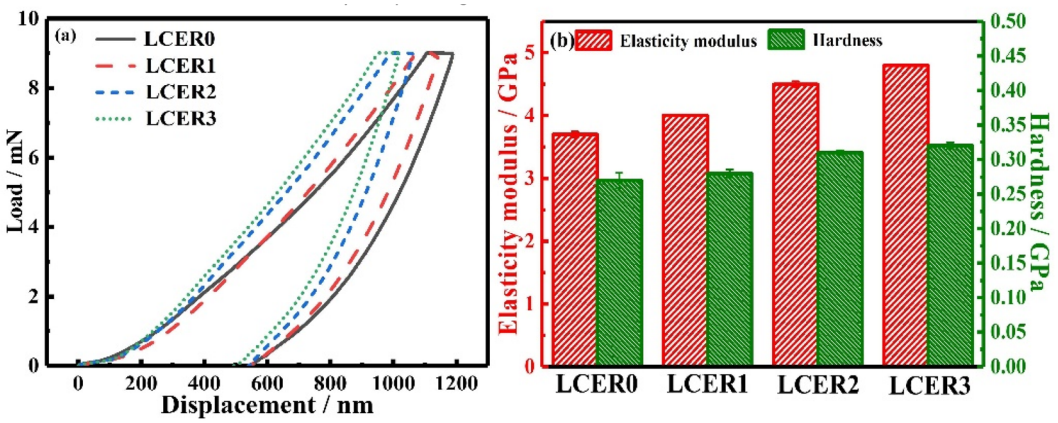

Fig. 7 (a) Load–displacement curves and (b) elastic modulus and hardness of LCERs.

increasing the content of BLCM, as shown in Fig. 7b. The elastic modulus and hardness of LCER3 are increased to 4.8 and 0.32 GPa, respectively, which are 30% and 19% higher than the values of LCER0, with an elastic modulus of 3.7 GPa and a hardness of 0.27 GPa. This is because the addition of BLCM introduces rigid biphenyl units into the crosslinked epoxy networks. Besides, the π–π stacking between biphenyl units strengthens the intermolecular force, which improves the regularity of the cured networks, thereby improving the indentation resistance, elastic modulus, and hardness of LCERs.

4. Conclusions

In summary, a biphenyl mesogen-containing co-curing agent (BLCM) was synthesized by a facile one-step condensation reaction and characterized by NMR, HRMS, and FT-IR. POM, WAXD, and SAXS demonstrated that the stacking of biphenyl mesogens promoted the formation of locally ordered regions in the liquid crystalline epoxy resins (LCER) network. Besides, the crystallinity of LCERs increased when raising the content of BLCM, resulting in an enhanced intrinsic thermal conductivity. When the mass fraction of BLCM was 60% of E-51 (LCER3), λ increased to 0.42 W (m K)$^{-1}$, which was 2.1 times that of an epoxy resin cured using DDM only (LCER0), with a λ of 0.20 W (m K)$^{-1}$. Besides, LCER3 presented both high thermal stability and mechanical properties. The heat resistance index, elastic modulus, and hardness were 176.8 °C, 4.8 GPa, and 0.32 GPa, respectively, also higher than the values of LCER0 with a heat resistance index of 172.2 °C, elastic modulus of 3.7 GPa, and hardness of 0.27 GPa. This work applies a commercially available epoxy to prepare epoxy resins with enhanced intrinsic thermal conductivities and is expected to provide a facile and convenient approach for the preparation of highly intrinsic thermally conductive polymeric materials.

Author contributions

The manuscript was written through contributions of all authors. All authors have given approval to the final version of the manuscript.

Conflicts of interest

There are no conflicts to declare.

Acknowledgements

The authors are grateful for support and funding from the Guangdong Basic and Applied Basic Research Foundation (2019B1515120093), National Natural Science Foundation of China (51773169), and China Postdoctoral Science Foundation (2022T150530). M. K. Li acknowledges the Undergraduate Innovation & Business Program of Northwestern Polytechnical University. This work is also financially supported by the Polymer Electromagnetic Functional Materials Innovation Team of Shaanxi Sanqin Scholars. The authors would also like to thank Dr Xuke Li from Ningbo University for help with the WAXD and SAXS measurements.

References

1 J. Wan, J. Zhao, X. Zhang, H. Fan, J. Zhang, D. Hu, P. Jin and D.-Y. Wang, *Prog. Polym. Sci.*, 2020, **108**, 101287.
2 A. V. Pansare, S. R. Khairkar, A. A. Shedge, S. Y. Chhatre, V. R. Patil and A. A. Nagarkar, *Adv. Mater.*, 2018, **30**, 1801523.
3 C. Huang, J. Peng, S. Wan, Y. Du, S. Dou, H. D. Wagner, A. P. Tomsia, L. Jiang and Q. Cheng, *Angew. Chem., Int. Ed.*, 2019, **58**, 7636–7640.
4 D. An, X. Duan, S. Cheng, Z. Zhang, B. Yang, Q. Lian, J. Li, Z. Sun, Y. Liu and C.-P. Wong, *Composites, Part A*, 2020, **135**, 105928.
5 L. Guo, Z. Zhang, M. Li, R. Kang, Y. Chen, G. Song, S.-T. Han, C.-T. Lin, N. Jiang and J. Yu, *Compos. Commun.*, 2020, **19**, 134–141.
6 Y. Han, K. Ruan and J. Gu, *Nano Res.*, 2022, **15**, 4747–4755.
7 T. Na, S. Che, Y. Sun, X. Liu, J. Hao and C. Zhao, *J. Appl. Polym. Sci.*, 2019, **136**, 47078.
8 A. Yu, P. Ramesh, X. Sun, E. Bekyarova, M. E. Itkis and R. C. Haddon, *Adv. Mater.*, 2008, **20**, 4740–4744.
9 Z. Xing, W. Sun, L. Wang, Z. Yang, S. Wang and G. Liu, *J. Mater. Sci.*, 2019, **54**, 10041–10054.
10 Y. Feng, G. Han, B. Wang, X. Zhou, J. Ma, Y. Ye, C. Liu and X. Xie, *Chem. Eng. J.*, 2020, **379**, 122402.
11 J. He, H. Wang, Q. Qu, Z. Su, T. Qin, Y. Da and X. Tian, *Compos. Commun.*, 2020, **22**, 100448.
12 S. Liu, B. Zhao, L. Jiang, Y.-W. Zhu, X.-Z. Fu, R. Sun, J.-B. Xu and C.-P. Wong, *J. Mater. Chem. C*, 2018, **6**, 257–265.
13 F. Xu, Y. Cui, D. Bao, D. Lin, S. Yuan, X. Wang, H. Wang and Y. Sun, *Chem. Eng. J.*, 2020, **388**, 124287.
14 D. Mao, J. Chen, L. Ren, K. Zhang, M. M. F. Yuen, X. Zeng, R. Sun, J.-B. Xu and C.-P. Wong, *Composites, Part A*, 2019, **123**, 260–269.
15 M. Rafiee, F. Nitzsche, J. Laliberte, S. Hind, F. Robitaille and M. R. Labrosse, *Composites, Part B*, 2019, **164**, 1–9.
16 Z. Liu, Y. Chen, Y. Li, W. Dai, Q. Yan, F. E. Alam, S. Du, Z. Wang, K. Nishimura, N. Jiang, C.-T. Lin and J. Yu, *Nanoscale*, 2019, **11**, 17600–17606.
17 J. Luo, X. Yang, R. Tusiime, H. Chen, Y. Liu, H. Zhang and J. Yu, *Compos. Commun.*, 2022, **29**, 101044.
18 Z. Tian, J. Sun, S. Wang, X. Zeng, S. Zhou, S. Bai, N. Zhao and C.-P. Wong, *J. Mater. Chem. A*, 2018, **6**, 17540–17547.
19 J. Hu, Y. Huang, Y. Yao, G. Pan, J. Sun, X. Zeng, R. Sun, J.-B. Xu, B. Song and C.-P. Wong, *ACS Appl. Mater. Interfaces*, 2017, **9**, 13544–13553.

20 Y. Ouyang, L. Bai, H. Tian, X. Li and F. Yuan, *Composites, Part A*, 2022, **152**, 106685.
21 H. Ma, B. Gao, M. Wang, Z. Yuan, J. Shen, J. Zhao and Y. Feng, *J. Mater. Sci.*, 2021, **56**, 1064–1086.
22 A. Kumar, K. Sharma and A. R. Dixit, *Carbon Lett.*, 2021, **31**, 149–165.
23 Q. Gao, Y. Pan, G. Zheng, C. Liu, C. Shen and X. Liu, *Adv. Compos. Hybrid Mater.*, 2021, **4**, 274–285.
24 Z. Wang, M. Yang, Y. Cheng, J. Liu, B. Xiao, S. Chen, J. Huang, Q. Xie, G. Wu and H. Wu, *Composites, Part A*, 2019, **118**, 302–311.
25 J. E. Peters, D. V. Papavassiliou and B. P. Grady, *Macromolecules*, 2008, **41**, 7274–7277.
26 R. Haggenmueller, C. Guthy, J. R. Lukes, J. E. Fischer and K. I. Winey, *Macromolecules*, 2007, **40**, 2417–2421.
27 J. Han, G. Du, W. Gao and H. Bai, *Adv. Funct. Mater.*, 2019, **29**, 1900412.
28 Y. Zhang and S.-J. Park, *Polymer*, 2019, **168**, 53–60.
29 X. Zhong, K. Ruan and J. Gu, *Research*, 2022, **2022**, 9805686.
30 Y. Li, J. Gao, X. Li, X. Xu and S. Lu, *Polymers*, 2018, **10**, 485.
31 Y.-S. Lin, S. L.-C. Hsu, T.-H. Ho, S.-S. Cheng and Y.-H. Hsiao, *Polym. Eng. Sci.*, 2017, **57**, 424–431.
32 Q. Zhang, G. Chen, K. Wu, J. Shi, L. Liang and M. Lu, *J. Appl. Polym. Sci.*, 2020, **137**, 49143.
33 X. Zhong, X. Yang, K. Ruan, J. Zhang, H. Zhang and J. Gu, *Macromol. Rapid Commun.*, 2022, **43**, 2100580.
34 X. Yang, X. Zhong, J. Zhang and J. Gu, *J. Mater. Sci. Technol.*, 2021, **68**, 209–215.
35 J. Maire, R. Anufriev, R. Yanagisawa, A. Ramiere, S. Volz and M. Nomura, *Sci. Adv.*, 2017, **3**, e1700027.
36 X. Yang, C. Liang, T. Ma, Y. Guo, J. Kong, J. Gu, M. Chen and J. Zhu, *Adv. Compos. Hybrid Mater.*, 2018, **1**, 207–230.
37 M. Akatsuka and Y. Takezawa, *J. Appl. Polym. Sci.*, 2003, **89**, 2464–2467.
38 W. Solodenko, G. Jas, U. Kunz and A. Kirschning, *Synthesis*, 2007, 583–589.
39 S. Xu, J. Cai, X. Qin, D. Wang, T. Bai and F. Sun, *Packag. Eng.*, 2016, **37**, 99–102.
40 M. Ghaemy, H. Behmadi and M. Barghamadi, *J. Appl. Polym. Sci.*, 2007, **106**, 4060–4066.
41 V. L. Zvetkov, *Polymer*, 2001, **42**, 6687–6697.
42 K. Ruan and J. Gu, *Macromolecules*, 2022, **55**, 4134–4145.
43 T. Giang and J. Kim, *Liq. Cryst.*, 2016, **629**, 12–26.
44 T. Giang and J. Kim, *J. Electron. Mater.*, 2017, **46**, 627–636.
45 W. Chen, K. Wu, Z. Tan and M. Lu, *Polym. Int.*, 2020, **69**, 346–354.
46 M. M. Hossain, A. I. Olamilekan, H.-O. Jeong, H. Lim, Y.-K. Kim, H. Cho, H. D. Jeong, M. A. Islam, M. Goh, N.-H. You, M. J. Kim, S. Q. Choi, J. R. Hahn, H. Yeo and S. G. Jang, *Macromolecules*, 2022, **55**, 4402–4410.
47 S. J. Yuan, Z. Q. Peng, M. Z. Rong and M. Q. Zhang, *Mater. Chem. Front.*, 2022, **6**, 1137–1149.
48 K. Ruan, Y. Guo and J. Gu, *Macromolecules*, 2021, **54**, 4934–4944.